Cu-Zn disorder and band gap fluctuations in $Cu_2ZnSn(S,Se)_4$: theoretical and experimental investigations

Jonathan J.S. Scragg [*,1], Jes K. Larsen[1], Mukesh Kumar[2], Clas Persson[3], Jan Sendler[4], Susanne Siebentritt[4] and Charlotte Platzer Björkman[1]

[1] Ångström Solar Center, Solid State Electronics, Uppsala University, Box 534, SE-751 21 Uppsala, Sweden.
[2] Environmental Remediation Materials Unit, National Institute for Materials Science, Ibaraki 305-0044, Japan
[3] Department of Physics, University of Oslo, P. O. Box 1048 Blindern, NO-0316 Oslo, Norway.
[4] Laboratory for photovoltaics, Physics and Materials Science Research Unit, University of Luxembourg, 41 rue du Brill, 4422 Belvaux, Luxembourg

* Corresponding author: e-mail jonathan.scragg@angstrom.uu.se, Phone: +46 (0) 18 471 3382

$Cu_2ZnSn(S,Se)_4$ (CZTS(e)) solar cells suffer from low open circuit voltages that have been blamed on the existence of band gap fluctuations, with different possible origins. In this paper we show, from both theoretical and experimental standpoints, that disorder of Cu and Zn atoms is in all probability the primary cause of these fluctuations. First, quantification of Cu-Zn disorder in CZTS thin films is presented. The results indicate that disorder is prevalent in the majority of practical samples used for solar cells. Then, *ab initio* calculations for different arrangements and densities of disorder-induced [Cu_{Zn} + Zn_{Cu}] defect pairs are presented and it is shown that spatial variations in band gap of the order of 200 meV can easily be caused by Cu-Zn disorder, which would cause large voltage losses in solar cells. Experiments using Raman spectroscopy and room temperature photoluminescence combined with in-situ heat-treatments show that a shift in the energy of the dominant band-to-band recombination pathway correlates perfectly to the order-disorder transition, which clearly implicates Cu-Zn disorder as the cause of band gap fluctuations in CZTS. Our results suggest that elimination or passivation of Cu-Zn disorder could be very important for future improvements in the efficiency of CZTS(e)-based solar cells.

1 Introduction Cu_2ZnSnS_4 (CZTS) is being studied intensively for future application in thin film photovoltaic (PV) solar cells. Due to the abundance of all constituent elements, it is potentially a low cost, sustainable solution for multi-terawatt levels of PV deployment. At present, efforts are focussed on bringing the power conversion efficiency (PCE) of CZTS devices to commercially interesting levels – in the range 15-20% – from the current record level of 12.6% (for a device also containing selenium) [1]. For even the best solar cells, the factor limiting the PCE at present is the open circuit voltage, $V_{oc,}$ which remains much lower than could be expected given the band gap of CZTS, which is about 1.5 eV [2,3]. The evidence suggests that part of the V_{oc} loss is due to non-optimal band alignment with the CdS buffer layer. This is true for CZTS, but not for the selenide equivalent, $Cu_2ZnSnSe_4$ (CZTSe) [4]. However, since large voltage deficits are observed in both materials, this cannot be the full explanation. Device modelling showed that band gap fluctuations, by causing a substantial reduction in the effective band gap, could account for a range of measured behaviours, including the low V_{oc}. These band gap fluctuations were attributed to a high density of compensated defects of unspecified type [5]. This explanation is consistent with the widespread observation that the band-to-band transition in the room temperature photoluminescence (RT-PL) spectrum occurs at energies several hundred meV below the fundamental band gap, i.e. 1.3-1.35 eV for CZTS [2,6,7]. Different causes of fluctuations in the band gap have been proposed, such as inclusions of stannite [2,8] or the presence of [Cu_{Zn}^{-}+Sn_{Zn}^{2+}] defect complexes [6]. The aim of this paper is to demonstrate that the true explanation for large, voltage-limiting band gap fluctuations in CZTS(e) is the existence of Cu-Zn disorder in the crystal structure, a phenomenon that is in all probability ubiquitous in the current generation of CZTS(e) films. Thus, we identify a critical problem that needs to be tackled to drive future improvements in CZTS(e) solar cell efficiency.

2 Cu-Zn disorder in CZTS(e) CZTS(e) crystallises in the kesterite structure, in which the planes at z = ¼ and z = ¾ contains only Cu and Zn atoms [9,10]. Cu-Zn disorder arises because of facile atomic exchange within these planes (between the 2*c* and 2*d* positions, using Wyckoff notation), while the rest of the lattice is undisturbed [11]. Fig. 1 shows the relevant lattice sites and planes in the

kesterite structure and illustrates the disorder-free and fully-disordered cases.

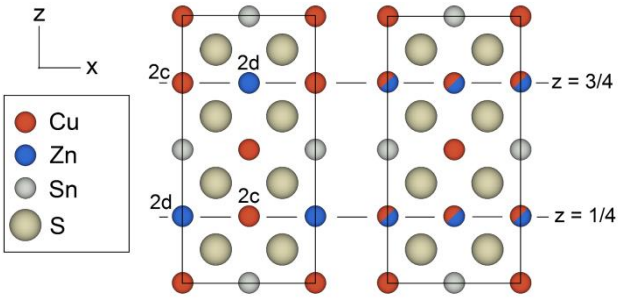

Figure 1. Projections of the conventional kesterite unit cell along the *y*-axis, indicating the atoms, lattice planes and lattice sites involved in Cu-Zn disorder. The fully disordered case is shown on the right, in which the Cu and Zn atoms in the z = ¼ and ¾ planes have a random distribution among the 2*c* and 2*d* sites.

Since Cu-Zn disorder is difficult to detect, especially in thin films, it can be easily overlooked in CZTS samples used for solar cells. But, it is governed by some relatively well-understood physics, and the amount of Cu-Zn disorder in a given sample is dependent primarily on its thermal history. Therefore, we can use the existing data to *estimate* how much disorder is present in a given case, as will be covered briefly here.

The amount of disorder is quantified by the long range order parameter, *S*, which ranges from 1, for perfect order, to 0, for total disorder:

$$S = \frac{\mathrm{P(Cu_{2c})} - a_{2c}}{1 - a_{2c}} = 2\mathrm{P(Cu_{2c})} - 1 = 2\mathrm{P(Zn_{2d})} - 1 \quad (1)$$

$\mathrm{P(Cu_{2c})}$ is the probability that a Cu atom occupies its native 2*c* site, which decreases from 1 for perfect order to 0.5 in completely disordered material. a_{2c} is the fraction of 2*c* sites in the z = ¼, ¾ lattice planes, equal to 0.5. For stoichiometric material, $\mathrm{P(Cu_{2c})} = \mathrm{P(Zn_{2d})}$. Of particular interest is the function $S_e(T)$, the order parameter of a sample that has reached equilibrium at a temperature T. This function is determined by the balance of the enthalpic and entropic contributions of disorder to the structural free energy, and it gives the maximum value of S (i.e., the greatest possible amount of order) that can be achieved in a sample at a given ambient temperature. Whether this maximum is actually reached depends on the rate at which Cu and Zn cations can exchange positions, which slows rapidly at lower temperatures [12]. S_e is 0 (total disorder) above the "critical temperature" of the order-disorder transition (~260°C for CZTS [11] and ~200°C for CZTSe [13]), increases rapidly just below this temperature, and then at lower temperatures rises gradually towards its maximum value of 1 (perfect order), which, it should be stressed, is theoretically only possible at 0 K. Fig. 2 shows some examples of $S_e(T)$ curves.

In general, experimental S values can be determined by X-ray diffraction methods, but in CZTS(e) this is complicated since Cu^+ and Zn^{2+} have the same scattering factors [10]. However, recently Rey et al. showed that the band gap of CZTSe acts as a reasonable *secondary* order parameter – i.e. it is roughly proportional to S if other important variables are constant [13]. This allowed a determination of $S_e(T)$ for CZTSe by fitting to a version of the kinetic model for the order-disorder-transition developed by Vineyard [14]. This model gave rate constants k_O and k_D for the ordering and disordering processes as:

$$k_O = 4f\exp\left(\frac{-U}{k_bT}\right)\exp\left(\frac{3vS}{k_bT}\right)$$

$$\text{and} \quad k_D = 4f\exp\left(\frac{-U}{k_bT}\right)\exp\left(\frac{-3vS}{k_bT}\right) \quad (2)$$

$$\text{where} \quad \frac{dS}{dt} = \frac{1}{2}\left[k_O(1-S)^2 - k_D(1+S)^2\right] \quad (3)$$

f is the frequency of the vibrational mode by which neighbouring atoms are exchanged (set to 1 THz as representative of a typical lattice vibration), U is the activation energy for the exchange process and v relates to the interaction energies of the three possible nearest neighbour pairs (Cu-Cu, Zn-Zn and Cu-Zn) [13]. The quantity $3vS/k_bT$ is positive for k_O and negative for k_D. The $S_e(T_e)$ curve published by Rey et al. for CZTSe is shown in Fig. 2.

Previously, we showed that the near-resonant Raman spectrum of CZTS can provide a qualitative measure of disorder, via the intensity ratio Q of the two A-modes at ~290 and ~305 cm^{-1} [11]. Following the example of Rey et al., we fitted this data to Vineyard's model (with an additional point at 110°C coming from this study). A linear correlation between S and Q was assumed, i.e., $Q = mS + c$. The value adopted by Q above the critical temperature, where S = 0, provides the constant c, and m was a fitting parameter. Numerical integration of Equation (3) was performed, iterating until dS/dt became negligible, at which point $S = S_e$. Values for the fit parameters were as follows: U/k_b = 14900 K, v/k_b = 358 K, m = 2.51 and c = 0.57. As noted by Rey et al [13], the values of U and f are not accurate since they cannot be determined independently of one another in this treatment. The quality of the fit, shown in Fig. 2, indicates that Q, like the band gap, can function as a reasonable secondary order parameter. This means that S values can relatively easily be estimated for thin film samples, since the resonant Raman spectrum is straightforward to obtain. It is apparent that CZTS has a higher equilibrium ordering at given T than CZTSe, which is reasonable since the critical temperature is higher (260 c.f. 200°C). We caution that Fig. 2 should not be used to determine S values for samples which deviate substantially in composition or preparation

method from those used here, due to the influence of sample composition and the type of non-stoichiometry on the Raman measurement [15].

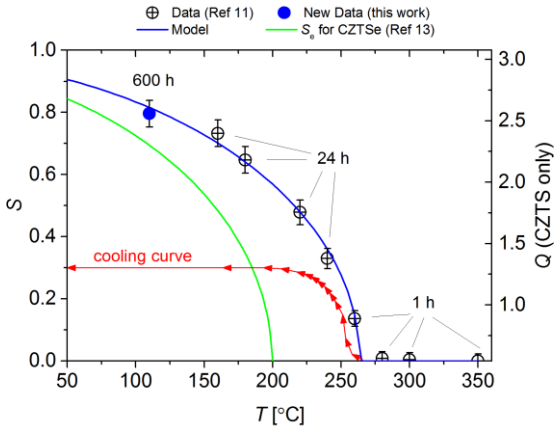

Figure 2. Long range order parameters, *S*, at equilibrium for Cu_2ZnSnS_4 (CZTS, this work) and $Cu_2ZnSnSe_4$ (CZTSe, Ref. [13]). *S* goes to zero at the critical temperature for the respective materials. Right axis: the Raman-derived parameter, *Q* which acts as a secondary order parameter. The red curve indicates schematically the evolution of order during post-synthesis cooling of a CZTS sample. Labels indicate the anneal times used to reach equilibrium at the given temperature.

From Fig. 2, we know the upper limit to the order parameter at a given temperature. If this limit is reached, the sample has come to equilibrium at that temperature. For the data points in Fig. 2, equilibrium was reached by extended post annealing of the samples. In normal solar cell processing, the relatively high cooling rates provide insufficient time for equilibrium to be reached, with the result that once the sample gets to room temperature it has excess disorder "frozen" into it ($S < S_e$). This is indicated qualitatively by the "cooling curve" in Fig. 2. Based on the time taken to reach the various equilibrium points in Fig. 2, we anticipate that typical "solar cell grade" CZTS(e) will have *S*-values from 0.1 (for rapid-thermally processed samples such as ours [16]) to 0.4 (for a tube furnace-type system with passive cooling).

Disorder and *S*-values can also be discussed in terms of point defects, because disorder consists of Cu_{Zn} or Zn_{Cu} substitutions in the kesterite lattice. In fact, since these defects have effective charges and the formation of defect pairs, $[Cu_{Zn}+Zn_{Cu}]$, is highly favourable [17], it is reasonable to assume that disorder creates such defect pairs rather than independent point defects. We can define the *average* number of $[Cu_{Zn}+Zn_{Cu}]$ pairs in each conventional kesterite unit cell, $D_{[CZ]}$, in terms of *S*:

$$D_{[CZ]} = 2(1 - P(Cu_{2c})) = 1 - S \qquad (4)$$

Typical *S* and $D_{[CZ]}$ values for different CZTS(e) processes are summarised in Table 1. For the highest reported *S* values to date – those in the upper part of Fig. 2 – we have on average 0.2-0.3 defect pairs *in each unit cell*. For typical levels of ordering, as mentioned above, $D_{[CZ]}$ can reach values in the range of 0.6-0.9 per unit cell. This translates to a volumetric defect density of $2\text{-}3\times10^{21}$ cm^{-3}. An important distinction must be made here. In discussing defects in solar cell materials, we typically talk of much lower concentrations, e.g. 10^{16}-10^{18} cm^{-3}, which is equivalent to one defect in 1000-100,000 unit cells. In that case we consider the defects as introducing discrete energy levels into the band gap (see e.g. [18]). However, at the concentrations discussed here, this treatment is probably not valid, and instead it is more realistic to consider the defects as a structural modification that perturbs the fundamental band gap itself. This is the standpoint taken here and in some other cases (e.g. refs [17,19]).

Table 1. Measured and estimated *S*-values and $[Cu_{Zn}+Zn_{Cu}]$ defect numbers per unit cell in different kinds of $Cu_2ZnSnS(e)_4$ samples.

Sample	*S*	$D_{[CZ]}$	Measurement of *S*	Source
Slow-cooled CZTS	0.4	0.6	Neutron scattering	[10]
CZTS equilibrated at 110°C	0.8	0.2	Raman	This work
CZTSe equilibrated at 100°C	0.7	0.3	Optical band gap	[13]
"Typical" CZTS(e) - rapid thermal process	0.2	~0.8	Estimate based on our baseline process	[11]
"Typical" CZTS(e) - tube furnace process	0.3-0.4	0.6-0.7	Estimated	

3 Band gap calculations for kesterite structures with various defect densities In this section we consider how strongly Cu-Zn disorder could influence the band gap in CZTS(e). Based on the literature, the answer to this question is not immediately obvious. The presence of one $[Cu_{Zn}+Zn_{Cu}]$ defect pair in a 128-atom kesterite supercell (equivalent to $D_{[CZ]} = 0.125$) yielded band gap narrowing of ~40 meV, and the conclusion that this defect was benign [20]. However, compared to the defect densities just described, this value of $D_{[CZ]}$ is unrealistically low. At the other extreme, ordered structures with one defect pair per unit cell ($D_{[CZ]} = 1$) have been examined by Paier et al [19]. Their $P\bar{4}2c$ structure had formation energy only 0.3 meV/atom higher than kesterite, but again, a limited band gap narrowing of 30

meV. An intermediate case, with one defect in a 64-atom supercell ($D_{[CZ]}$ = 0.25), yielded much greater band gap narrowing of 110 meV [21]. To get a clearer picture of the variation in band gap for a large range of defect densities, we simulated 64-atom supercells containing different numbers of [Cu_{Zn}+Zn_{Cu}] defects in different arrangements. The considered cases include exchange of both nearest-neighbour Cu and Zn atoms as well as exchange of atoms from neighbouring Cu-Zn planes. Up to four such exchanges were considered per supercell, and the minimum and maximum energy structures were calculated in each case. The PBE functional was used for formation energy calculations, but since this approach tends to yield near-zero band gap values for the Kesterite (and also the Chalcopyrite) system, the HSE06 functional was used to get a more reliable indication of band gap variations. It is noted that the use of a supercell assumes that the defects are arranged in an infinitely repeating ordered fashion, which is of course not realistic – in a disordered material the defect arrangement must by definition vary spatially. The different modelled supercells simply represent some of the defect arrangements that could occur in localised regions within a grain of disordered CZTS. The treatment of a disordered material as a "summation" of many different, coexisting ordered structures is well established and discussed in e.g. Ref [22]. There are many more possible defect arrangements that cannot be simulated in the confines of a 64-atom supercell, but the ones chosen here give an idea of the range of variation of the important parameters. Full calculation details and figures showing some simulated atomic arrangements are given in the supporting information to this paper. The calculation results are shown in Table 2, with the appropriate $D_{[CZ]}$ values.

First, we focus on the variation of formation energy for the highest and lowest energy defect arrangements. For $D_{[CZ]}$ up to 0.5 defect pairs per unit cell, the formation energy increases and is similar regardless of the defect arrangement. After that, the formation energy diverges: the formation energy for $D_{[CZ]}$ = 0.75 or 1 depends strongly on the particular arrangement the defects adopt: the minimum energy is reduced for some arrangements and increased for others. This divergence is due to the interaction of nearby defects. The lowest energy structures at each defect density contain [Cu_{Zn}+Zn_{Cu}] pairs aligned with each other within one Cu-Zn lattice plane in the supercell. This minimises the number of "incorrect" nearest-neighbour interactions (i.e. Cu-Cu, Zn-Zn), thus lowering the overall energy. The higher energy structures are those with defect pairs in different lattice planes or isolated Cu_{Zn} and Zn_{Cu} defects. We note that for $D_{[CZ]}$ = 1, the minimum energy arrangement corresponds to the $P\bar{4}2c$ structure simulated by Paier et al, and the associated energies are in good agreement (see Table 2).

Table 2. Calculations for structures with various [Cu_{Zn}+Zn_{Cu}] defect densities, expressed by $D_{[CZ]}$, the number of defect pairs per conventional kesterite unit cell. ΔE_f and ΔE_g are the formation energy in meV/atom and the band gap shift in meV with respect to perfect kesterite. The upper part of the table gives literature data. The lower part of the table contains the defect arrangements modelled in this work. The label KS64_*x.xx*L/H indicates a 64-atom kesterite supercell with $D_{[CZ]}$ equal to *x.xx*. L/H indicates the Lowest/Highest energy configuration at the given defect density.

Structure	$D_{[CZ]}$	ΔE_f	ΔE_g	Source (note)
Kesterite	0	0	0 (E_g = 1.5 eV)	[17,19]
$P\bar{4}2c$ CZTS	1	0.3	-29	[19]
128-atom supercell	0.125	1.6	-40	[20]
64-atom supercell	0.25	4.1	-110	[21]
KS64_0.00L	0	0	0	(Kesterite)
KS64_0.25L	0.25	3.3	-114	
KS64_0.25H	0.25	3.7	-141	
KS64_0.50L	0.5	4.7	-157	
KS64_0.50H	0.5	5.0	-205	
KS64_0.75L	0.75	3.4	-127	
KS64_0.75H	0.75	12	-255	
KS64_1.00L	1	0.30	-24.0	($P\bar{4}2c$ CZTS)
KS64_1.00H	1	17	-305	(PMCA CZTS)

The reduction of formation energy for higher defect densities in certain arrangements is significant, because it points to the formation of clusters of [Cu_{Zn}+Zn_{Cu}] defect pairs (as also shown elsewhere [21]). Cluster formation by definition introduces spatial variations in defect density, which is a necessary condition if Cu-Zn disorder is to explain the observed spatial band gap fluctuations in CZTS.

Fig. 3 shows the band gap shift with respect to kesterite as a function of the formation energy for the various defect arrangements in Table 2. There is in general a good correlation between formation energy and band gap shift, with the band gap becoming narrower for the defect arrangements with higher formation energy. For the lower energy structures, the dependence is reasonably linear, as indicated in the figure. It is apparent that large band gap shifts are possible for structures with modest formation energies – e.g. around 150-200 meV for ΔE_f = 5 meV/atom, which may reasonably be expected to occur in experimental samples (especially given the favourable entropy of introducing disorder). Combining this with the spatially varying defect density implied by disorder and defect clustering, the outcome is that Cu-Zn disorder ought to yield substantial spatial variations in the band gap in typical CZTS samples. In terms of the possible effect on the open circuit voltage in a solar cell, Werner et al showed (for a Cu(In,Ga)Se_2, rather than CZTS absorber) that band gap fluctuations with standard deviation in the range of just

125 meV led to V_{oc} losses of 260 mV for an average band gap of 1.15 eV [23]. Larger fluctuations will have an increasingly drastic effect.

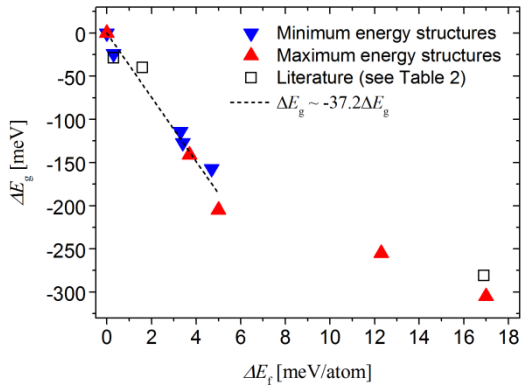

Figure 3. Band gap shift relative to kesterite plotted against the formation energy of the various defect arrangements shown in Table 2, indicating an approximately linear correlation for lower formation energies.

4 Experimental observations of disorder-dependent band gap fluctuations. We have seen from a theoretical perspective that large band gap fluctuations could be introduced at the typical [Cu_{Zn}+Zn_{Cu}] defect densities that are associated with Cu-Zn disorder. In the final section, we use experimental means to confirm that the band gap fluctuations responsible for the dominant radiative recombination channel observed in CZTS samples are indeed strongly linked to the amount of Cu-Zn disorder.

4.1 Experimental CZTS films were prepared according to our baseline reactive sputtering and annealing procedure [16]. XRF measurements on the sputtered precursors gave composition ratios Cu/Sn = 1.9 and Cu/Zn = 1.6. After annealing, comparisons using EDS (due to smaller sample size) showed that there was minimal change in composition. This composition lies within the CZTS + ZnS two-phase region of the pseudo-ternary phase diagram [24]. UV-Raman measurements (not shown) confirmed ZnS secondary phases at the sample surface, but no other secondary phases were observed by Raman spectroscopy with a 532 nm excitation. A Renishaw inVia system was used for all Raman and room temperature photoluminescence (RT-PL) measurements. The laser spot size was estimated to be about 5µm.

Samples were induced to become highly ordered by further annealing at 110°C for 600-900 hours in a N_2 atmosphere. Raman spectra of the resulting ordered material with 785 nm excitation – see Fig. 4 – were fitted with 11 Lorentzian peaks based on known phonon modes of CZTS (see e.g. Ref. [25]) to extract the intensities of the individual modes. From these, the value of Q was determined to be 2.55, which yields an S-value of ~0.8, confirming that a high degree of ordering was reached. In the near-resonant spectrum for ordered material, the higher frequency modes can be used to evaluate the stoichiometry type, using the peak ratio $Q' = I_{340}/(I_{369}+I_{377})$ [15]. A value near 2, as here, indicates so-called B-type stoichiometry, i.e. that the Zn-rich composition of the CZTS phase is accommodated by the presence of [$2Zn_{Cu}$+Zn_{Sn}] defect pairs. These defects have no interaction with [Cu_{Zn}+Zn_{Cu}] [15], and have minimal influence on the band gap in the relevant concentration range [20], meaning that the calculations in Section 2, which were made for stoichiometric material, are applicable to our non-stoichiometric experimental samples.

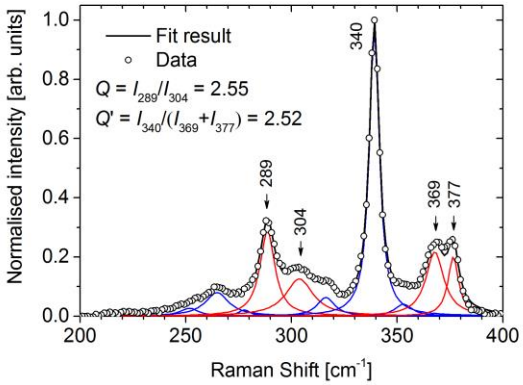

Figure 4. Near-resonant Raman spectrum of a Cu_2ZnSnS_4 sample annealed for 900h at 110°C to induce ordering. The individual Lorentzian components of a full spectrum fit are indicated.

A piece of the highly ordered material was then loaded under a nitrogen atmosphere into a Linkam TMS600 thermal stage with quartz window, that was then mounted in the Raman/RT-PL measurement system. Raman and RT-PL measurements were repeated using excitation wavelengths of 785 nm (Raman only) and 532 nm (both techniques) to establish reference spectra in the thermal stage.

After that, a series of RT-PL and Raman measurement cycles were performed, using in-situ heating between measurements to transition the sample to a disordered state in a stepwise manner. Each heat treatment lasted for 20 minutes, and the sample was cooled to room temperature in between to perform measurements. The heating and cooling rates were 150°C/min, sufficiently fast for the sample to retain a level of disorder characteristic of the heating temperature. The heating temperatures were, in the order performed, T = 180, 240, 265, 275, 280, 300 and 350°C i.e. approaching and then exceeding the critical temperature of the order-disorder transition (T_c = 260°C). For the final four steps, the sample should be completely disordered, and undergo no further changes, since $T > T_c$. The entire series of measurements and heating steps were

performed in a single, continuous run at the same spot on the sample, and optical images showed that drift was negligible. Thus, the absolute intensity of the Raman and PL signals can be compared throughout the experiment.

4.2 Results Normalised Raman spectra with 785 nm excitation are shown as a function of heat treatment temperature in Fig. 5(a). A rapid drop in spectral intensity as the sample becomes more disordered (not shown) indicates a decrease in the resonance effect. This is expected, because the band gap ought to get smaller with decreasing order [13,26], becoming further from the excitation wavelength (785 nm ≡ 1.58 eV). Meanwhile, the non-resonant spectrum, using the 532 nm laser, is unchanged.

Values of the order parameter, *S*, were calculated from the resonant Raman spectra for each treatment temperature using the method described above and in previous work [11]. *S* decreased in the expected manner, dropping to zero near the critical temperature.

Fig. 5(b) shows normalised RT-PL spectra during the heat treatment series. The presence of multiple peaks is apparent; however, these coincide with interference fringes in the reflectance spectrum, so we ascribe them to a measurement artefact (this is discussed in detail in Ref. [27]). As illustrated in the supporting information, the interference fringes can be mathematically removed from the spectrum where measured or simulated reflectance spectra are available. For our samples, a roughly Gaussian PL peak is obtained. Despite the interference effect, the trend in peak position seen in Fig. 5(b) is clear: there is a large red shift as *S* decreases.

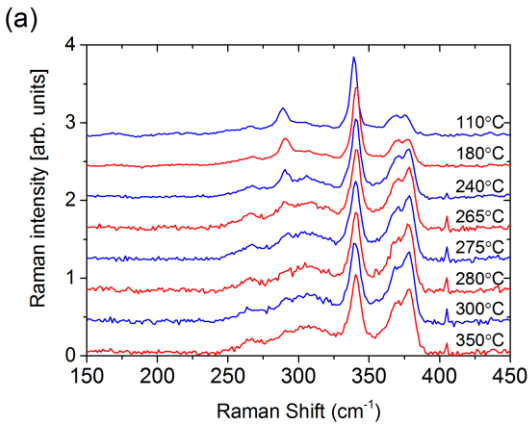

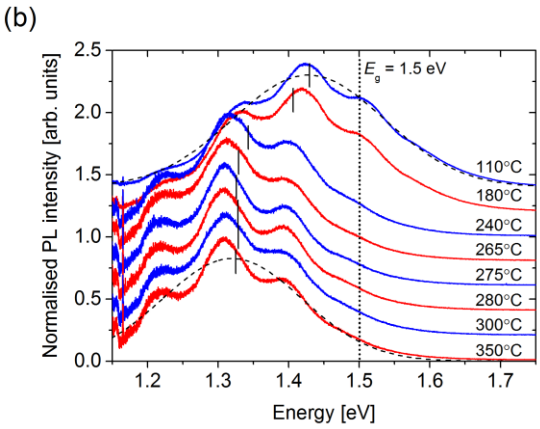

Figure 5 (a) Raman spectra with 785nm excitation wavelength recorded during the order-disorder transition. The temperature at which the sample was equilibrated prior to each measurement is indicated; the measurements were made at room temperature. (b) Corresponding room-temperature photoluminescence spectra. Note that interference effects cause the "ripples" in the spectra. Example Gaussian fits (which closely approximate the actual PL response, see Ref. [27]) are shown for the 110°C and 350°C spectra, and the fitted peak positions are indicated by the vertical dashes.

To determine the nature of the transitions in the RT-PL spectra, excitation-intensity-dependent measurements at room temperature were made for ordered (S ~ 0.8) and disordered (S ~ 0) pieces of the same sample: see Fig. 6.

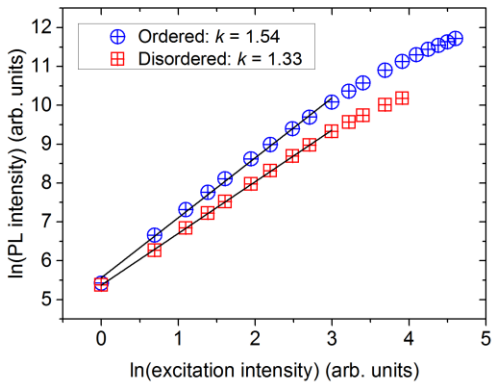

Figure 6 Dependence of RT- PL intensity on excitation intensity for ordered and disordered pieces of a Cu_2ZnSnS_4 sample. The straight lines indicate the regions of data from which the *k*-factors were calculated.

The data follow a power-law relationship, $I_{PL} \propto I_{exc}^{k}$, over at least three orders of magnitude, yielding *k*-factors of 1.54 and 1.33 in the ordered and disordered pieces, respectively. *k* factors greater than 1 indicate that the PL corresponds to band-to-band (BB) transitions [28,29]. The slightly lower *k*-factor for the disordered piece again indicates higher non-radiative recombination.

The fact that the RT-PL peak at ~1.3-1.4 eV corresponds to a BB transition means that the dominant pathway for carriers to undergo radiative recombination is a band gap that is lower than the fundamental band gap of CZTS by several hundred meV. This is not a new observation, see e.g. [6,7,30], and, like the low V_{oc}, it is generally explained by the existence of spatial potential fluctuations in the band structure (band gap or electrostatic potential fluctuations – see e.g., Ref. [23]). Interestingly, though, the energy of the BB transition appears to change in response to the heat treatments applied to our samples. This is clear in Fig 7, where the RT-PL peak positions (BB transition energies) from the data in Fig. 5(b) are shown as a function of heat treatment temperature. Also shown are the corresponding *S* values calculated from the Raman data according to the method described earlier. There is a remarkable correlation between the BB transition energy and the order parameter, *S*: both parameters drop rapidly as the critical temperature for the order-disorder-transition is reached, and are constant thereafter. In the most ordered sample (*S* ~0.8), the BB transition energy reaches 1.43 eV. It is supposed that if ordering could be further improved, the peak would climb to the energy of the fundamental band gap, ~1.5 eV.

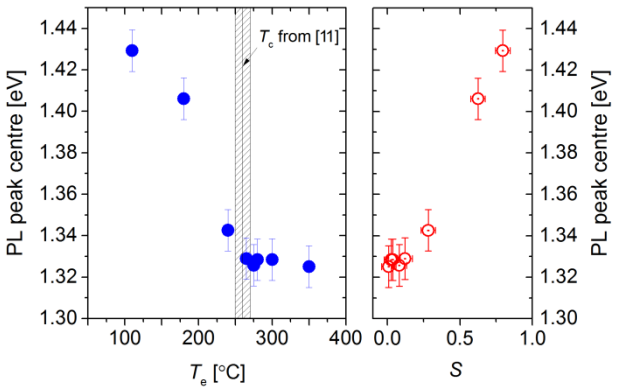

Figure 7. The RT-PL peak position throughout the order disorder transition, plotted as a function of equilibration temperature, T_e, and order parameter, *S*. *S*-values were calculated from the Raman spectra of Fig. 5(a).

This, then, is direct evidence that Cu-Zn disorder is responsible for the band gap fluctuations that give the low BB transition energy in CZTS. None of the other explanations proposed for the band gap fluctuations, the presence of secondary phases, inclusions of stannite [2,8] or the presence of $[Cu_{Zn}^{-}+Sn_{Zn}^{2+}]$ defects [6] – could possibly account for the observed behaviour, especially the agreement of the critical temperature for the order-disorder transition with the point at which the RT-PL stops changing. The magnitude of the band gap fluctuations described in the previous section is also in good agreement with the RT-PL results. In the most disordered case, the BB peak in RT-PL is about 200 meV below the fundamental band gap, which we showed could be occasioned by $[Cu_{Zn}+Zn_{Cu}]$ defect arrangements having formation energy of ~5 meV/atom. In Fig. 3 we showed the positive correlation between the formation energy of defect arrangements and their band gap narrowing effect. It is reasonable to suppose that in more ordered samples – i.e. those that have reached equilibrium at lower temperatures – only defect arrangements with lower formation energies can exist. Thus, the magnitude of band gap fluctuations is expected to decrease as the sample becomes more ordered, and the BB peak will increase in energy, exactly as observed. It also follows that the energy of the BB transition might be used to estimate the state of Cu-Zn disorder in a given sample, all other things being equal. In the literature, this peak usually occurs in the region of 1.3-1.35 eV [2,6,7], which, from Fig. 7, translates to *S*-values in the range 0-0.4. This is precisely the range that was anticipated in the introduction for typical CZTS(e) samples prepared for solar cells, on the basis of the kinetics of the order-disorder transition. This agreement underlines the fact that the majority of experimental samples CZTS(e) contain high levels of Cu-Zn disorder.

If Cu-Zn disorder is indeed as widespread as we predict, band gap fluctuations and their knock-on-effects such as low open circuit voltage will be a problem for CZTS(e) from all manner of production processes – which is certainly the case. Unfortunately, the basic physics of the order-disorder transition and the low critical temperatures for CZTS and CZTSe suggest that disorder is inherently difficult to reduce much beyond what we have achieved in this work, due to the slow kinetics of ordering. As an extreme example, a hypothetical CZTS(e) module, which may have an operating temperature around 50°C in normal conditions, could not have an *S*-value of more than 0.8-0.9 (according to Fig. 1), and only after an impractically long time at the operating temperature would this level finally be reached. If we cannot eliminate disorder itself, then "passivation" approaches are required to reduce its effects. One intriguing possibility is based on the introduction of other defect types that interact with $[Cu_{Zn}+Zn_{Cu}]$. For example, Paris et al, showed that "A-type" defects, $[V_{Cu}+Zn_{Cu}]$, were connected with lower levels of disorder for a given preparation process [15]. Calculations have reached a related conclusion: A-type defects appear to aggregate with $[Cu_{Zn}+Zn_{Cu}]$, reducing the structural energy and, furthermore, counteracting the reduction in band gap [21]. These results suggest that the presence of A-type non-stoichiometry might not only limit the amount of

disorder, but also reduce the depth of band gap fluctuations. It is notable that recent efficiency records have been achieved with compositions in the A-type region [31,32], and have exhibited PL peak energies that nearly matched the band gap, along with improved open circuit voltages, suggesting the elimination of large band gap fluctuations. To the best of our knowledge, it is not yet known how to deliberately form A type CZTS(e). Investigation of this, and the inclusion of other defects, both intrinsic and extrinsic, that might have similar influences, could lead to some useful "defect engineering" approaches to improve the properties of CZTS(e) and the resulting solar cell efficiencies.

5 Conclusions Our results show that disorder among the Cu and Zn atoms in the kesterite structure is a critical contribution to the band gap fluctuations that have been blamed for the large voltage deficit in CZTS(e) solar cells. Disorder causes a very high density of [Cu_{Zn}+Zn_{Cu}] defect pairs, the precise concentration depending on the thermal history (i.e. synthesis method) of the sample in a more-or-less predictable way. We show that a substantial concentration of [Cu_{Zn}+Zn_{Cu}] defects will always occur in practical samples even when considerable efforts are made to reach high ordering. *Ab initio* calculations reveal two important features: first that at the anticipated defect densities, clustering of [Cu_{Zn}+Zn_{Cu}] pairs is favourable. This will lead to a spatially varying defect distribution. Second, that the defect density is sufficient to cause a significant reduction of the effective band gap, leading to the prediction that disorder will introduce spatial band gap fluctuations in the range of several hundred meV. This would cause drastic losses in open circuit voltage, and therefore efficiency, in a solar cell. Room temperature photoluminescence data show a strong correlation between the energy of the dominating band-to-band recombination pathway and the state of Cu-Zn ordering, allowing us to propose that Cu-Zn disorder is the primary cause of band gap fluctuations in CZTS(e). Control of disorder could then be a key route to improving the performance of this technology, and some approaches to tackling this problem were briefly mentioned.

Acknowledgements JJSS would like to acknowledge Vetenskapsrådet for funding. CP acknowledges support from the Norwegian Research Council (contract 243642) and HPC resources at USIT through NOTUR. Part of this work (JS) has been funded by the Marie Curie Initial Training Network "Kestcells", project number FP7-PEOPLE-2012-ITN.316488

References

[1] Wei Wang, Mark T. Winkler, Oki Gunawan, Tayfun Gokmen, Teodor K. Todorov, Yu Zhu, and David B. Mitzi, Advanced Energy Materials **4** (7), 10.1002/aenm.201301465 (2014).

[2] Susanne Siebentritt and Susan Schorr, Progress in Photovoltaics: Research and Applications **20** (5), 512 (2012).

[3] David B. Mitzi, Oki Gunawan, Teodor K. Todorov, and D. Aaron R. Barkhouse, Philosophical Transactions of the Royal Society A **371: 20110432**, DOI: 10.1098/rsta.2011.0432 (2013).

[4] Alex Redinger, Marina Mousel, Max Hilaire Wolter, Nathalie Valle, and Susanne Siebentritt, Thin Solid Films **535**, 291 (2013).

[5] Tayfun Gokmen, Oki Gunawan, and David B. Mitzi, Appl. Phys. Lett. **105** (3), 033903 (2014).

[6] M. Grossberg, T. Raadik, J. Raudoja, and J. Krustok, Current Applied Physics **14** (3), 447 (2014).

[7] Hui Du, Fei Yan, Matthew Young, Bobby To, Chun-Sheng Jiang, Pat Dippo, Darius Kuciauskas, Zhenhuan Chi, Elizabeth A. Lund, Chris Hancock, Win Maw Hlaing OO, Mike A. Scarpulla, and Glenn Teeter, J. Appl. Phys. **115** (17), 173502 (2014).

[8] Rabie Djemour, J. Appl. Phys. **116** (7), 073509 (2014).

[9] L. Choubrac, M. Paris, A. Lafond, C. Guillot-Deudon, X. Rocquefelte, and S. Jobic, Physical Chemistry Chemical Physics **15** (26), 10722 (2013).

[10] S. Schorr, Solar Energy Materials and Solar Cells **95** (6), 1482 (2011).

[11] J. J. S. Scragg, L. Choubrac, A. Lafond, T. Ericson, and C. Platzer-Bjorkman, Appl. Phys. Lett. **104** (4), 041911 (2014).

[12] W. L. Bragg and E. J. Williams, Phil. Trans. R. Soc. A **145** (855), 699 (1934).

[13] G. Rey, A. Redinger, J. Sendler, T. P. Weiss, M. Thevenin, M. Guennou, B. El Adib, and S. Siebentritt, Appl. Phys. Lett. **105** (11), 112106 (2014).

[14] G. H. Vineyard, Phys. Rev. **102** (4), 981 (1956).

[15] M. Paris, L. Choubrac, A. Lafond, C. Guillot-Deudon, and S. Jobic, lnorg. Chem. **53** (16), 8646 (2014).

[16] Jonathan J. Scragg, Tomas Kubart, J. Timo Wätjen, Tove Ericson, Margareta K. Linnarsson, and Charlotte Platzer-Björkman, Chemistry of Materials **25** (15), 3162 (2013).

[17] Shiyou Chen, X. G. Gong, Aron Walsh, and Su-Huai Wei, Appl. Phys. Lett. **94** (4), 041903 (2009).

[18] Ling Yin, Guanming Cheng, Ye Feng, Zhaohui Li, Chunlei Yang, and Xudong Xiao, RSC Advances **5** (50), 40369 (2015).

[19] Joachim Paier, Ryoji Asahi, Akihiro Nagoya, and Georg Kresse, Physical Review B **79** (11), 115126 (2009).

[20] Shiyou Chen, Aron Walsh, Xin-Gao Gong, and Su-Huai Wei, Advanced Materials **25** (11), 1522 (2013).

[21] Dan Huang and Clas Persson, Thin Solid Films **535**, 265 (2013).

[22] ShunLi Shang, Yi Wang, Greta Lindwall, Neal R. Kelly, Timothy J. Anderson, and Zi-Kui Liu, The Journal of Physical Chemistry C (2014).
[23] Jürgen H. Werner, Julian Mattheis, and Uwe Rau, Thin Solid Films **480–481** (0), 399 (2005).
[24] I. D. Olekseyuk, I. V. Dudchak, and L. V. Piskach, J. Alloys Compd. **368** (1-2), 135 (2004).
[25] M. Dimitrievska, A. Fairbrother, X. Fontané, T. Jawhari, V. Izquierdo-Roca, E. Saucedo, and A. Pérez-Rodríguez, Appl. Phys. Lett. **104** (2), 021901 (2014).
[26] Carlos Rincón, Physical Review B **45** (22), 12716 (1992).
[27] J. K. Larsen, S.-Y. Li, J. J. S. Scragg, Y. Ren, C. Hägglund, M. D. Heinemann, S. Kretzschmar, T. Unold, and C. Platzer-Björkman, J. Appl. Phys. **118** (3), 035307 (2015).
[28] S. Siebentritt, *Wide Band Gap Chalcopyrites*. (Springer, Berlin, Heidelberg, New York, 2006).
[29] T. Schmidt, K. Lischka, and W. Zulehner, Physical Review B **45** (16), 8989 (1992).
[30] M. Grossberg, J. Krustok, T. Raadik, M. Kauk-Kuusik, and J. Raudoja, Current Applied Physics **14** (11), 1424 (2014).
[31] G. Brammertz, M. Buffière, S. Oueslati, H. ElAnzeery, K. Ben Messaoud, S. Sahayaraj, C. Köble, M. Meuris, and J. Poortmans, Appl. Phys. Lett. **103** (16), 163904 (2013).
[32] Yun Seog Lee, Talia Gershon, Oki Gunawan, Teodor K. Todorov, Tayfun Gokmen, Yudistira Virgus, and Supratik Guha, Advanced Energy Materials, doi: 10.1002/aenm.201401372 (2014).